

An Improved Method to Calculate Cerebral Metabolic Rates of Glucose Using PET

Robert L. Phillips, Caroline Y. Chen, Dean F. Wong and Edythe D. London

Neuroimaging and Drug Action Section, Intramural Research Program, National Institute on Drug Abuse, National Institutes of Health, Bethesda, Maryland; Department of Radiology, Johns Hopkins University School of Medicine, Baltimore, MD; and Department of Pharmacology and Experimental Therapeutics, School of Medicine, University of Maryland, Baltimore, Maryland

PET methods for single-scan measurement of the cerebral metabolic rate of glucose (CMR_{glc}) generally involve sampling of radioactivity in arterial plasma over the course of the experiment. The purpose of this study was to develop an analytic procedure that would require substantially fewer plasma samples to measure CMR_{glc} using the single-scan method. **Methods:** This technique uses a model for the curve describing the time course of radioactivity in plasma. **Results:** This model obviates the need to draw arterial samples at short time intervals or at all during the first 30 min after radiotracer injection. The new technique uses six samples to provide the same accuracy and precision as the conventional method provides with 30 or more samples. **Conclusion:** The proposed method greatly simplifies quantitative PET studies of glucose metabolism.

Key Words: positron emission tomography; cerebral glucose metabolism; fluorodeoxyglucose; brain

J Nucl Med 1995; 36:1668-1679

The autoradiographic 2-deoxy-D-1-[¹⁴C]glucose method to determine the cerebral metabolic rate of glucose (CMR_{glc}) was developed for use in laboratory animals over a decade ago (1). The technique was later extended to studies using PET and the radiotracers 2-[¹⁸F]fluoro-2-deoxy-D-glucose (FDG) and 2-deoxy-D-1-[¹¹C]glucose in humans and subhuman primates (2-5).

To calculate CMR_{glc}, autoradiographic and PET deoxyglucose methods require the following measurements:

1. Radioactivity in tissue at a time when radiotracer uptake is essentially complete, usually 45 min or more after the injection of radiotracer.
2. Concentration of glucose in arterial plasma.
3. Concentration of radiotracer in arterial plasma (C_p), at multiple times (t) from injection of the radiotracer until measurement of radioactivity in tissue.

The time course of C_p (i.e., C_p(t)) is the input function for a calculation of expected concentration of radiotracer in the tissue of interest. An operational equation is used to calculate CMR_{glc} from these values using rate constants for the transport, phosphorylation and dephosphorylation of the radiotracer and an estimate of the relative predilection of the brain to take up and phosphorylate the radiotracer as compared with glucose (3).

Calculations of CMR_{glc} traditionally integrate C_p(t) numerically. The set of values of C_p(t) are subject to a variety of errors that can cause one or more of the samples in the set to differ from their correct values. Samples of C_p(t) can also be missing from the set. Numeric integration techniques generally contain no mechanism to reduce the effect of a small number of errant data values. To reduce the effects of such errors, an analytically integrable function can be fitted to the values of C_p(t). The fitting process, if properly done using a suitable function, can reduce the effect of the incorrect or missing data points on the value of the integral. Some equations that are used for this purpose include two-, three-, and four-term linear exponentials and sums of *gamma* functions (3,4,6,7). Techniques that fit C_p(t) to a function may reduce the variance in measurements of CMR_{glc}. Such techniques, however, rely on measurement of the entire time course of C_p and therefore are no simpler than numeric integration techniques.

There have been attempts to calculate metabolic rates for glucose in the heart without sampling the entire time course of C_p. Values of cardiac glucose metabolism calculated by the Patlak method are highly correlated with those of a simple index of FDG uptake (% dose/100 ml tissue) (8). This index can be determined without blood sampling. It is, however, sensitive to uncontrollable factors, such as the levels of glucose and insulin in plasma.

Calculation of CMR_{glc} can be based on an integration that is generated by averaging several curves of C_p(t) to form a population-average curve (9). To correct for differences in the dose administered and in the body mass of the subject, the population-average curve can be normalized to

Received Mar. 17, 1994; revision accepted Sept. 20, 1994.

For correspondence or reprints contact: Robert L. Phillips, PhD, Neuroimaging and Drug Action Section, National Institute on Drug Abuse Addiction Research Center, P.O. Box 5180, Baltimore, MD 21224.

match the activity of two different samples of $C_{p_n}(t)$.^{*} Values of CMR_{glc} calculated by numerically integrating the normalized population average curve of $C_p(t)$ correlate well with those calculated by the conventional method. This method is less sensitive to uncontrolled factors (see above) than the previous method. It does, however, require a highly standardized injection protocol; and, as shown below, it also may be sensitive to differences in tracer clearance rates.

The purpose of this study was to develop a model to predict CMR_{glu} by fitting $C_p(t)$ using a small number of plasma samples. Ideally, the process would be insensitive to variance in injection technique and to uncontrollable factors, such as concentrations of insulin and glucose in plasma, and to tracer clearance rates.

This article addresses the following six questions:

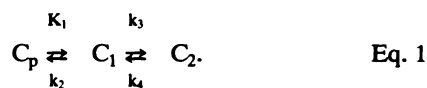
1. Is there sufficient information within a small subset of samples of $C_{p_n}(t)$ to predict CMR_{glc}?
2. What analytic function best represents the curve of $C_p(t)$?
3. How many adjustable parameters are required in the function?
4. How sensitive is the calculation to the shape or magnitude of the "peak" or maximum amount of radioactivity in plasma?
5. How sensitive is the calculation to aberrant samples?
6. What is the minimum number of plasma samples required?

MATERIALS AND METHODS

Theory

Models generally used for measuring metabolic rates for glucose have three compartments and four rate constants. The compartments and their forward and reverse rate constants are defined as follows: C_p , the plasma compartment; C_1 , the compartment directly coupled to plasma and governed by facilitated transport of the radiotracer in tissue; C_2 , the compartment containing labeled phosphorylated metabolite (2-[¹⁸F]fluoro-2-deoxy-D-glucose-6-phosphate). The forward rate constants are K_1 and k_3 . The reverse rate constants are k_2 and k_4 .

The phosphorylated metabolite remains inside the cell for a relatively long time because it cannot readily cross the cell membrane, nor is it a suitable substrate for further glycolysis. Dephosphorylation is slow since it requires the enzyme glucose-6-phosphatase, which is not abundant in the brain or heart. Schematically, the model is represented as follows:



^{*}The terms $C_p(t)$, $C_1(T)$ and $C_2(T)$ refer to concentrations of radiotracer (as FDG or its metabolite), in the corresponding compartment, as a function of time after injection (t or T). The terms $C_p(t_x)$, $C_1(T_x)$, and $C_2(T_x)$ indicate concentrations evaluated or measured at the specific times t_x or T_x . The values of radioactivity in samples of plasma are referred to as $C_{p_n}(t)$. The subscript n denotes the (ordinal) number of the sample. The time, after injection of radiotracer, at which the sample was drawn is t . When the notation C_x is used, the subscript x can take on either of the values 1 or 2. Thus, $C_x(T_x)$ means the values of either function, $C_1(T_x)$ or $C_2(T_x)$, evaluated at the time T_x .

We can derive equations for the three-compartment model as follows:

$$\frac{dC_1}{dt} = K_1 C_p(t) - (k_2 + k_3)C_1(t) + k_4 C_2(t) \quad \text{Eq. 2}$$

$$\frac{dC_2}{dt} = k_3 C_1(t) - k_4 C_2(t).$$

The solution is given by the following integral equations:

$$C_1(T) = \frac{K_1}{(\alpha_2 - \alpha_1)} [(k_4 - \alpha_1)e^{-\alpha_1 T} - (k_4 - \alpha_2)e^{-\alpha_2 T}] \otimes C_p(t) \quad \text{Eq. 3A}$$

$$C_2(T) = \frac{K_1 K_3}{(\alpha_2 - \alpha_1)} [e^{-\alpha_1 T} - e^{-\alpha_2 T}] \otimes C_p(t), \quad \text{Eq. 3B}$$

where T is the time of measurement of radioactivity in tissue (e.g., by PET scan). Given $C_1(T)$ and $C_2(T)$, CMR_{glc} may be estimated by any of several operational equations (3, 10, 11). The symbol \otimes represents convolution and α_1 and α_2 (the characteristic eigenvalues of the differential equation system) are defined as follows:

$$\alpha_1 = \frac{(k_2 + k_3 + k_4) - \sqrt{(k_2 + k_3 + k_4)^2 - 4k_2 k_4}}{2}$$

$$\alpha_2 = \frac{(k_2 + k_3 + k_4) + \sqrt{(k_2 + k_3 + k_4)^2 - 4k_2 k_4}}{2} \quad \text{Eq. 4}$$

The letter t refers to time after injection of FDG. All measures of radioactivity are decay-corrected to the time of injection of the radiotracer. The following values of the rate constants were used: $K_1 = 0.102 \text{ min}^{-1}$, $k_2 = 0.13 \text{ min}^{-1}$, $k_3 = 0.062 \text{ min}^{-1}$ and $k_4 = 0.0068 \text{ min}^{-1}$ (3). The values of $C_1(T)$ and $C_2(T)$, together with the amount of radioactivity in the tissue ($C(T)$) are entered into an operational equation such as that of Huang et al.:

$$r\text{CMR}_{\text{glc}} = \frac{C_p}{L_c} \frac{K_1 k_3}{(k_2 + k_3)} \frac{C_1(T) - C_1(T)}{C_2(T)}, \quad \text{Eq. 5}$$

that relates metabolic rate to the measurements.

Development and Testing of the Model

Development of the model required sequential investigation of the questions posed in the introduction. Each question was answered in a separate step that entailed a specific series of analyses. The results of each step were used to modify the approach taken subsequently. Steps 1 through 3 defined the actual model, whereas steps 4 through 6 examined its sensitivity to specific perturbations.

1. Is There Sufficient Information within a Small Subset of Samples of $C_{p_n}(t)$ to Predict CMR_{glc}? The first task in this study was to demonstrate the possibility of the existence of a model that could accurately represent the integral of $C_p(t)$ (implicit in Eqs. 3 and 4) from a small number of samples of $C_{p_n}(t)$. Because of the formulation given in Equation 5, accurate estimation of $C_x(T)$ would yield accurate estimation of CMR_{glc}. As we reasoned that the nature of any correlation between $C_x(T)$ and $C_p(t)$ would provide evidence for the existence of a useful model, we performed a series of correlations between $C_x(T_x)$ and $C_p(t_x)$.

Values of $C_p(t_x)$ were calculated at a fixed set of times by linear interpolation using the measured values of $C_{p_n}(t)$ from human

PET studies (see below). The sets of times (T_i and t_k) ranged from 500 to 6000 sec in 500-sec intervals. The dataset in each correlation analysis consisted of values of $C_x(T_i)$ calculated by numeric integration to one of the times T_i , paired with values of $C_p(t_k)$. The analyses encompassed all possible pairs of times (T_i, t_k). Since it was important to determine which samples of $C_p(t)$ have useful information about the calculated values of $C_x(T)$, correlations between numerically calculated values of $C_x(T_i)$ vs. the largest observed value of $C_p(t)$ were also calculated.

The regression analysis used a linear correlation (i.e., an attempt to fit the calculated values of $C_x(T_i)$ to an equation) as follows:

$$C_x(T_i) = S_x(T_i, t_k)C_p(t_k) + I_x(T_i, t_k), \quad \text{Eq. 6}$$

in which $S_x(T_i, t_k)$ was the slope of the regression line, and $I_x(T_i, t_k)$ was the intercept. The behaviors of the slope ($S_x(T, t)$) and the intercept ($I_x(T, t)$) were important predictors of the utility of using a few samples of $C_p(t)$ to calculate $C_x(T)$. If the behavior were characterized by large random fluctuations, the only correct procedure for calculation of $C_x(T)$ would have been to perform the calculations of Equation 3 using numeric integration of the values from the samples of $C_p(t)$. If, on the other hand, the behaviors of $S_x(T, t)$ and $I_x(T, t)$ were smooth and predictable in both T and t , it would have been possible to use a simpler procedure for performing the calculations implicit in Equation 3.

The nature of the relationship between $S_x(T, t)$, T and t could most easily be displayed in three-dimensional surface plots. If any of $S_1(T, t)$, $S_2(T, t)$, $I_1(T, t)$ or $I_2(T, t)$ would have displayed large random fluctuations, the surface would also have fluctuated randomly. If the surface were smooth, the shape of the surface would have indicated the nature of the relationship between $C_x(T)$ and $C_p(t)$ and what form the analytic calculation of $C_x(T)$ from $C_p(t)$ would take. A flat surface would have indicated a linear relationship. If the surface were curved, but monotonic in T and t , the relationship would likely have been an exponential and/or a polynomial in T and t . If, on the other hand, the surface would have been nonmonotonic (i.e., contain "hills" and "valleys"), it would probably have been better to parameterize the essential portion of the curve described by actual measurements of $C_p(t)$. As shown below, a function which could be fitted to the values of samples of $C_p(t)$ was required. It was sought as the answer to the next question.

2. What Analytic Function Best Represents the Curve of $C_p(t)$?

A series of curve fitting experiments were conducted using different analytic functions. The objective was to select a function that accurately reproduced the results of numeric integration with the least sensitivity to aberrant samples, and the fewest adjustable parameters. The analyses used the following equations to fit each curve of $C_p(t)$:

$$C_p(t) = b_1 e^{-a_1 t} + b_2 e^{-a_2 t} \quad \text{Eq. 7}$$

and

$$C_p(t) = b_1 t e^{-a_1 t} + b_2 e^{-a_2 t}. \quad \text{Eq. 8}$$

In both equations, a_1 , a_2 , b_1 and b_2 were constants determined separately for each curve of $C_p(t)$ by a nonlinear least-squares fitting routine. Equation 7 was selected since it appeared in the literature as a suitable function for fitting the curve of $C_p(t)$ (4). The effects of adding additional terms to Equation 7 were also studied. The first extra term involved additional fitting parameters b_3 and a_3 in a manner exactly analogous to the use of parameters

b_2 and a_2 . Equation 8 was selected after a series of experiments involving subsets of the data showed that it fit all the curves with minimal residuals, and produced estimates of $C_x(T)$ that were insensitive to missing data in the curve of $C_p(t)$.

3. *How Many Adjustable Parameters Are Required in the Function?* Estimates were performed to determine how many parameters were required to evaluate $C_p(t)$ and its analytic integrals. It was reasoned that if the exponents and magnitudes (a and b) were proportional, then it would be possible to eliminate two of the four free parameters of Equations 7 and/or 8. The proportionality constants, m and n (see below), were derived from the entire dataset. After appropriate substitutions in Equation 8 (i.e., replacement of " a_1 " with " na ", " a_2 " with " a ", " b_1 " with " mb ", and " b_2 " with " b "), Equation 8 was written as follows:

$$C_p(t) = b[mte^{-nat} + e^{-at}]. \quad \text{Eq. 9}$$

4. How Sensitive Is the Calculation to the Shape or Magnitude of the "Peak" or Maximum Amount of Radioactivity in Plasma?

Studies were performed to test the sensitivity of the calculations of $C_1(T)$ and $C_2(T)$ to the magnitude of the peak $C_p(t)$. In these studies, differences between analytically and numerically derived estimates of $C_1(T_i)$ and $C_2(T_i)$ were correlated with magnitudes of the peak $C_p(t)$ both as the decay-corrected activity and as a normalized activity. Peak $C_p(t)$ was normalized by dividing it by the decay-corrected activity at 45 min (an arbitrary choice).

5. *How Sensitive Is the Calculation to Aberrant Samples?* To test the accuracy of the analytic technique, we studied the effect of aberrances in the curves of $C_p(t)$ on the calculation of $C_x(T_i)$. Correlation analysis was used to determine the causes of differences between results of calculations of $C_x(T_i)$ based on numeric integration and results of calculations of $C_x(T_i)$ based on analytic integration. The most useful correlation compared the percentage difference in the fit of Equation 9 to the values of $C_p(t)$ with the percentage difference in results of corresponding calculations of $C_x(T_i)$.

6. *What Is the Minimum Number of Plasma Samples Required?* Correlation analyses were performed to test the stability of the calculation of CMR_{glc} to the number of samples of $C_p(t)$ to which Equation 9 was fitted. Matrices of correlation coefficients were constructed between six sets of values of $C_x(T)$. The set of times to which the integration was performed were those times >20 min at which samples of $C_p(t)$ had been drawn during the corresponding PET study (see below). This choice eliminated endpoint corrections from the calculation.

Calculations of $C_x(T)$, as specified in Equation 3, were performed on the data from each PET study, using each of six possible functions as $C_p(t)$. These calculations generated six sets of values of $C_x(T)$. To obtain Set 1, all values of $C_p(t)$ were used, and the integration implicit in Equation 3 was performed by numeric methods. The other sets of values of $C_x(T)$ were calculated by performing the integration implicit in Equation 3 analytically. In the analytic calculations, the function $C_p(t)$ was based on Equation 9 with the coefficients (a and b) determined by fitting the equation to one of five subsets of values from each curve of $C_p(t)$.

In calculating Set 2 values of $C_x(T)$, the constants (a and b) in Equation 9 were determined by fitting the equation to all of the values from samples of $C_p(t)$ with $t > 20$ min. The calculation of the values of $C_x(T)$ in Set 3 started with the same set of samples of $C_p(t)$ as were used in the calculations for Set 1. The two samples of $C_p(t)$ with the largest residuals from the fit were

removed, however, and the fitting process was repeated to determine the constants (a and b) in Equation 9. In calculating the values of $C_x(T)$ from the remaining datasets (4, 5 and 6), the constants (a and b) in Equation 9 were determined by fitting the equation to the values in one of three different subsets of six samples of $C_{p_n}(t)$. After an initial curve fitting process, the two samples of $C_{p_n}(t)$ with the largest residuals were removed and the fitting process was repeated with four samples. The calculations of $C_x(T)$ in Set 4 used the first six samples of $C_{p_n}(t)$ with $t > 20$ min. The calculations of $C_x(T)$ in Set 5 used the last six samples of $C_{p_n}(t)$. The samples used to obtain Set 6 were spaced uniformly in time and were drawn >20 min but <90 min after injection of FDG.

Calculation

A routine was used numerically to integrate the time course of $C_{p_n}(t)$. It interpolated between each two adjacent time-activity points with a straight line, and analytically convolved this line with the appropriate exponential function. When the time of integration did not correspond exactly to the time at which a value of $C_{p_n}(t)$ had been measured, endpoint corrections were performed by linear interpolation of the value of $C_{p_n}(t)$ taken immediately before and the value taken immediately following the time T to which the integration was calculated.

Human Studies

Subjects for this study were human volunteers participating in PET measurements of CMRglc by the single-scan FDG method. All had physical examinations that showed various physiological parameters to be within normal limits. Diabetes, cardiovascular disease and renal dysfunction were among the exclusionary criteria of the protocols.

All subjects except one were male. The subjects ranged in age from 21 to 45 yrs (mean age = 31 yr). All subjects gave informed consent to the procedures in the protocols, which were approved by the institutional review boards of Johns Hopkins Medical Institutions and Francis Scott Key Medical Center, where the NIDA Intramural Research Program is located.

Data from 119 PET FDG studies of 61 subjects were used. Most of the studies tested acute effects of drug abuse on CMRglc. Subjects in these protocols underwent two PET studies, each involving administration of either placebo or an active drug, in random order and double-blind fashion. Of the 61 subjects, 20 were substance abusers enrolled in studies on the effects of cocaine HCl (40 mg intravenously) (12), 12 were involved in studies on the effects of morphine sulfate (30 mg intramuscularly) (13) and three participated in a study on the effects of buprenorphine HCl (1 mg intramuscularly) (14). Twenty-one subjects were normal controls. Of these, six received nicotine (1.5 mg intravenously) (15) and the remaining 15 received no drugs.

Five subjects with histories of polydrug abuse were studied in two other protocols. Four participated in a study in which two subjects who were physically dependent on opioids were maintained on heroin (7.5 mg subcutaneously four times per day). CMRglc (one measurement) in these subjects was compared with that in two subjects who were not physically dependent on opioids and who received no drug (16). One subject participated in a study on naloxone-precipitated opiate withdrawal. He underwent three PET studies, two of which were on the same day in a test-retest paradigm (17-19). While physically dependent on heroin, he received naloxone (0.4 mg intramuscularly) before the first measurement of CMRglc and morphine sulfate (15 mg intramuscularly) before the second. At the time of the third study, several weeks

later, no drug was administered and the subject had been detoxified.

All subjects received a standard nonketogenic breakfast on the day(s) of PET scanning (13). Subjects fasted for 3-7 hr and did not smoke for at least 2 hr prior to injection of FDG.

FDG for all studies was synthesized from [^{18}F]fluoride as described previously (20). Radiochemical purity of the product, determined using thin-layer chromatography or high-performance liquid chromatography, exceeded 98%. All preparations were determined to be sterile and pyrogen-free. FDG (nominally 185 MBq in 5.0 ml saline (all but one of the subjects) or 148 MBq in 5.0 ml saline (only the subject who received three PET scans) was infused manually, over 30 sec, through a catheter inserted into a vein in the forearm. Saline (20 ml) was infused after the FDG injection (13).

The PET scanner was a NeuroECAT with three rings of detectors (CTI, Knoxville, TN). Since the tomograph did not acquire data from the entire axial field of view in a single scan, a test session consisted of four scans of 15-min duration each; the subject was repositioned between scans. The first scan followed the injection of FDG by approximately 45 min. Repositioning the subject between scans required 2 to 5 min. Thus, the total duration of the study, from injection to end of the last PET scan, was approximately 2 hr.

Thirty to 35 blood samples were drawn manually through an indwelling radial arterial catheter, according to a schedule of decreasing frequencies starting at the time of FDG injection. The first eight samples were drawn at 15-sec intervals, then four at 30-sec intervals, two at 1-min intervals, four at 2-min intervals and two at 5-min intervals. Samples were then drawn at 10-min intervals until the subject was removed from the tomograph, at which time the final sample was drawn. The blood samples were centrifuged and aliquots of plasma were taken and counted in a well counter.

To calibrate the well counter with the tomograph, radioactivity in a uniform cylindrical phantom filled with a solution containing a positron-emitting isotope (nominally 74 MBq of ^{18}F or ^{68}Ga in approximately 4 liters of water) was measured in the PET scanner on each day that a study was performed. Aliquots of this solution were counted in the same well counter as the plasma samples.

RESULTS

Analysis of Linear Correlations

Correlation analysis of the calculated values of $C_x(T_i)$ versus $C_{p_n}(t_k)$ at fixed pairs of times (T_i, t_k) yielded a correlation coefficient $r > 0.89$ whenever $t_k > 15$ min and $T_i > 15$ min (Table 1, Fig. 1A, B). The mean (s.d.) of the correlation coefficients was 0.97 (0.02). There was little correlation between the calculated values of $C_x(T_i)$ versus peak $C_{p_n}(t)$ (Fig. 1C, D). Adding a second plasma sample to the relationship provided a small improvement (Table 2), as shown by a small decrease in the s.d. of the residuals (Fig. 2).

The high correlations observed in these calculations indicated that only one or, at most, two degrees of freedom would be required to predict values of $C_x(T)$ at any time T that exceeded 20 min after FDG injection. Standard deviations of the percentage residuals of these linear regressions were between 1% and 4%, but there were maximal percentage residuals of up to 20%.

TABLE 1
Correlation Coefficients Relating Numeric Calculation of $C_1(t)$ (A) and $C_2(t)$ (B) to $C_p(t)$ *

Scan time, T (min)	A. Sample time, t (min)								
	33.3	41.7	50.0	58.3	66.7	75.0	83.3	91.7	100.0
33.3	0.998	0.983	0.98	0.976	0.969	0.965	0.96	0.954	0.946
41.7	0.998	0.997	0.991	0.986	0.977	0.973	0.97	0.966	0.96
50.0	0.993	0.998	0.998	0.991	0.983	0.98	0.977	0.975	0.969
58.3	0.989	0.992	0.998	0.998	0.992	0.987	0.984	0.983	0.977
66.7	0.983	0.984	0.992	0.999	0.998	0.992	0.988	0.987	0.982
75.0	0.976	0.977	0.987	0.993	0.999	0.999	0.994	0.991	0.987
83.3	0.972	0.972	0.983	0.988	0.993	0.999	0.999	0.994	0.991
91.7	0.967	0.971	0.983	0.987	0.991	0.996	0.999	0.999	0.995
100.0	0.963	0.967	0.978	0.983	0.988	0.993	0.996	0.999	0.999

Scan time, T (min)	B. Sample time, t (min)								
	33.3	41.7	50.0	58.3	66.7	75.0	83.3	91.7	100.0
33.3	0.955	0.927	0.925	0.922	0.918	0.912	0.905	0.897	0.890
41.7	0.968	0.945	0.942	0.938	0.933	0.927	0.921	0.914	0.907
50.0	0.977	0.957	0.954	0.950	0.945	0.939	0.933	0.927	0.920
58.3	0.983	0.965	0.964	0.960	0.954	0.950	0.943	0.937	0.930
66.7	0.987	0.971	0.970	0.967	0.961	0.956	0.950	0.945	0.938
75.0	0.989	0.975	0.975	0.972	0.967	0.962	0.957	0.951	0.945
83.3	0.990	0.977	0.978	0.976	0.972	0.968	0.962	0.957	0.951
91.7	0.991	0.979	0.981	0.980	0.976	0.972	0.967	0.962	0.956
100.0	0.992	0.981	0.983	0.983	0.979	0.976	0.972	0.967	0.961

*One hundred seventeen data pairs were used for each correlation. The probability of finding so large a correlation coefficient by chance was <0.0001 for each pair of variables.

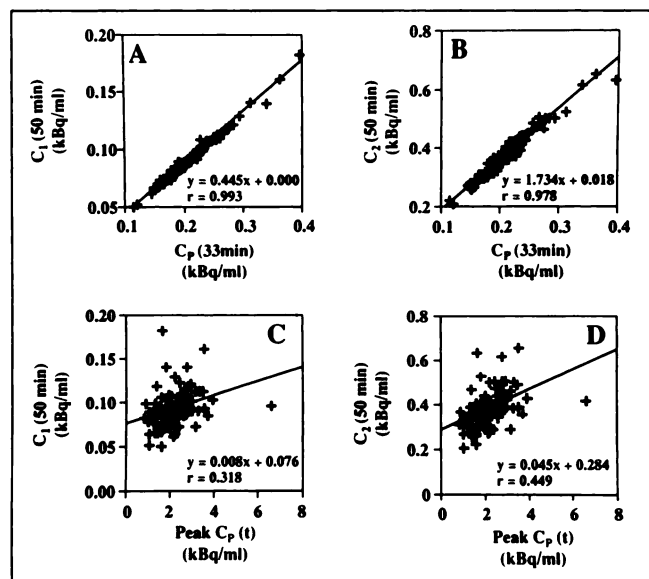


FIGURE 1. Typical plots showing the correlations of $C_x(T)$ (ordinates) with $C_p(t)$ (abscissas). (A) Correlation between $C_1(50 \text{ min})$ and $C_p(33 \text{ min})$. The correlation coefficient was 0.99. (B) Correlation between $C_2(50 \text{ min})$ and $C_p(33 \text{ min})$. The correlation coefficient was 0.98. (C) Correlation between $C_1(50 \text{ min})$ and the peak value of $C_p(t)$. (D) Correlation between $C_2(50 \text{ min})$ and the peak value of $C_p(t)$. The low correlations observed in panels C and D ($r = 0.32$ and $r = 0.45$, respectively) were typical of those obtained when $C_x(T)$ were correlated with the peak value of $C_p(t)$.

Three-dimensional surface plots of the slopes ($S_x(T_i, t_k)$) calculated in the regression analyses of $C_x(T_i)$ on $C_p(t_k)$ were smooth (Fig. 3), indicating that values of $C_x(T)$ (i.e. $C_1(T)$ and $C_2(T)$) could be predicted from individual samples of $C_p(t_k)$ (Fig. 3). The Y intercepts, $I_1(T_i, t_k)$ and $I_2(T_i, t_k)$, did not differ significantly from zero (data not shown).

If the surface had been flat and the maximal percentage errors had been consistently lower than 5%, we would have expressed the relationships between arbitrary values of $C_p_n(t)$ and calculated values of $C_x(T)$ as simple linear functions. If the surfaces had been monotonic, the relationship could have been expressed as either a sum of exponential functions or as a polynomial. The surfaces, while smooth, were neither flat nor monotonic in t or T . No satisfactory parameterization of the surface could be found. Such a parameterization would be essential for calculation of values of $C_x(T)$ whether from a single value of $C_p_n(t)$ or an average using several values. The shape of the surface and the values of the maximal percentage residuals supported the conclusion that parameterization of the curve of $C_p(t)$ was an appropriate approach to predict values of CMRglc.

Equation for Fitting $C_p_n(t)$

Equations 7 and 8 were used to fit each curve of $C_p(t)$ using only those values of $C_p_n(t)$ with $t > 20 \text{ min}$. There

TABLE 2
Results of Linear Correlation between $C_1(T)$ (A) and $C_2(T)$ (B) as the Dependent Variables with $Cp(t_1)$ and/or $Cp(t_2)$ as Independent Variables*

A									
T	t_1	t_2	adj r^2	r_1^2	r_2^2	max	min	mean	s.d.
33.3	33.3	peak	0.996	0.996	0.345	3.14	-3.62	-0.027	1.22
50.0	33.3	peak	0.987	0.986	0.318	7.88	-7.04	-0.055	2.45
58.3	58.3	peak	0.996	0.996	0.324	3.09	-4.67	-0.003	1.35
91.7	58.3	peak	0.968	0.966	0.333	6.76	-11.26	-0.109	3.65
33.3	33.3	58.3	0.996	0.996	0.953	3.32	-3.83	-0.032	1.12
58.3	33.3	58.3	0.998	0.978	0.996	2.43	-2.99	-0.003	1.00
91.7	33.3	58.3	0.975	0.935	0.974	6.52	-11.69	-0.107	3.64
B									
T	t_1	t_2	adj r^2	r_1^2	r_2^2	max	min	mean	s.d.
33.3	33.3	peak	0.947	0.912	0.490	10.45	-9.92	-0.222	4.48
50.0	33.3	peak	0.974	0.954	0.449	7.70	-7.49	-0.121	3.22
58.3	58.3	peak	0.938	0.922	0.436	15.88	-11.9	-0.265	5.34
91.7	58.3	peak	0.969	0.960	0.410	12.32	-8.39	-0.131	3.84
33.3	33.3	58.3	0.919	0.912	0.850	11.97	-14.26	-0.364	5.44
58.3	33.3	58.3	0.968	0.966	0.922	7.74	-8.11	-0.169	3.50
91.7	33.3	58.3	0.983	0.982	0.960	5.36	-6.36	-0.099	2.55

*The column labeled adj r^2 gives the adjusted r^2 for the bilinear fit, while the columns labeled r_1^2 and r_2^2 give the r^2 value found in separate linear regression analyses with $Cp(t_1)$ and $Cp(t_2)$, respectively, as independent variables. The columns labeled max and min give the maximum and minimum values for residual of the fit, as a percentage of the fitted value. The columns labeled mean and s.d. are the mean and standard deviation, respectively, of the percentage residuals. Addition of the sample with peak radioactivity did not improve the fit.

was no attempt to force the fit to accommodate the shape, magnitude or time of peak $Cp_n(t)$ because linear correlation studies (see above) indicated that early ($t < 20$ min) values of $Cp(t)$ were not correlated with $C_x(T_i)$. The fitted curve underestimated the value of $Cp_n(t)$ at peak by a factor of approximately three to four. The patterns of residuals from the fit of Equation 7 revealed many outliers. This finding indicated that the shape used for fitting was not optimal. The mean (s.d.) of the percentage residuals was 0.05% (3.7%) (Fig. 4A). The parameters were sensitive to elimination of data points from the fitting process. Addition of extra terms to Equation 7 provided flexibility in matching the shape of the fitted curve to the curve of $Cp_n(t)$, but it made the fitting process unstable. In contrast, the residuals from fitting Equation 8 to the curve of $Cp_n(t)$ were small. The mean (s.d.) of the percentage residuals was 0.03% (2.0%) (Fig. 4B).

Number of Parameters in the Equation for $Cp(t)$

Correlation plots of a_1 versus a_2 and of b_1 versus b_2 from all curves of $Cp_n(t)$ were prepared. The plots of results based on fitting Equation 7 to $Cp_n(t)$ indicated that a_1 and a_2 had some correlation, but that b_1 and b_2 did not. In contrast, the results calculated using Equation 8 showed that the exponents, a_1 and a_2 , were linearly related, as were the magnitudes, b_1 and b_2 (Fig. 5). The relationships were such that $a_1 \cong na_2$ and $b_1 \cong mb_2$, with $m = 0.0072 \text{ min}^{-1}$ and n

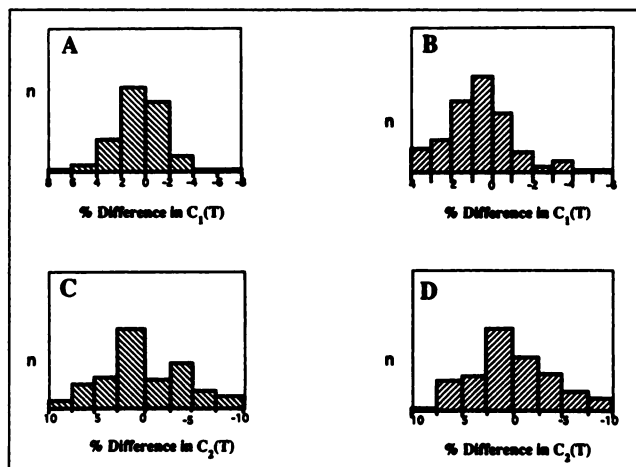


FIGURE 2. (A) Percentage difference in C_1 (30 min) calculated using numeric integration and using linear regression of C_1 (30 min) on Cp (30 min). The mean (s.d.) was -0.053% (2.45%). (B) Percentage difference between C_1 calculated using numeric integration and using bilinear regression of C_1 (30 min) on Cp (30 min) and Cp (60 min). The mean (s.d.) was -0.012% (1.72%). (C) Percentage difference between C_2 (30 min) calculated using numeric integration and linear regression of C_2 (30 min) on Cp (30 min). The mean (s.d.) was -0.22% (4.13%). (D) Percentage difference between C_2 (30 min) calculated using numeric integration and bilinear regression of C_2 (30 min) on Cp (30 min) and Cp (60 min). The mean (s.d.) was -0.21% (3.94%). Addition of a second sample of $Cp(t)$ in the regression analysis reduced the s.d.

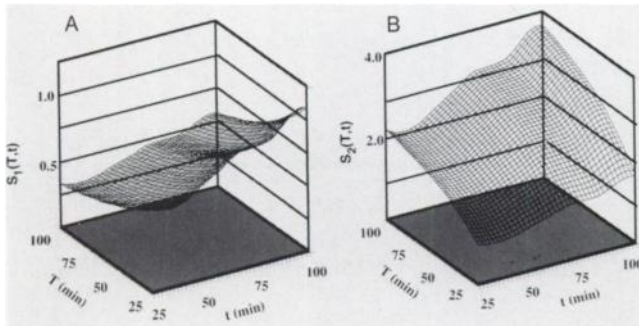


FIGURE 3. Three-dimensional surface plots of the slope from linear regression analyses of $C_1(T)$ on $C_p(t_k)$ (A) and $C_2(T)$ on $C_p(t_k)$ (B). The form of the regression was summarized in Equation 6 ($C_x(T_i) = S_x(T_i, t_k)C_p(t_k) + I_x(T_i, t_k)$). The values of $C_x(T_i)$ used in the linear regression were calculated by numeric integration of $C_p(t)$, as indicated in Equation 3. Ten values each of T_i and t_k were combined to give 100 measurements of $S_x(T_i, t_k)$ evenly distributed in time, starting at 25 min after injection and continuing until 100 min after injection of FDG. The surface regions between the measured values of $S_x(T_i, t_k)$ were generated by bi-cubic interpolation.

= 0.40. Replacing symbols in Equation 8 as follows gave Equation 9: “na” for “ a_1 ”, “a” for “ a_2 ”, “mb” for “ b_1 ”, and “b” for “ b_2 ”.

We obtained the percentage difference between the experimental and analytical curves of $C_p(t)$ using Equation 9. The s.d. of the differences was 2.2% and the mean was 0.027%. The s.d. was consistent with that given by calculations based on counting statistics in the well counter. The largest difference was less than 10% (Fig. 6). The coefficient of correlation between the measured value of $C_p(t)$ and that calculated from the equation was 0.99. Reducing the number of free parameters to one (by replacing the exponent “a” in Equation 9 by the mean “a” from all curves and fitting the resulting function to the curves of

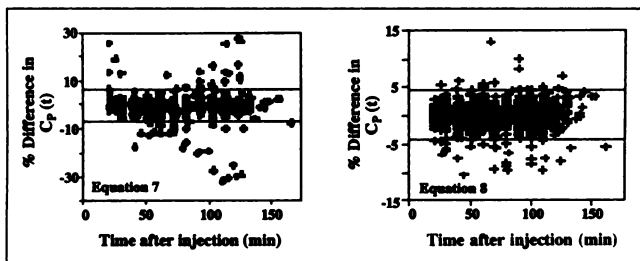


FIGURE 4. Percentage difference from fitting both Equations 7 (left) and 8 (right) to $C_p(t)$. The percentage differences were not always constant with time after injection, as indicated by curves deviating from being flat. Extreme outliers were visible after fitting Equation 7 with four free parameters. Note the different scale in the two panels. The range of values of differences from fitting Equation 7 was nearly twice as large as that found using Equation 8. Both the shape and the size of the differences from fitting Equation 7 to the values of $C_p(t)$ made it unreliable for predicting $C_x(T)$. In contrast, when the curve of $C_p(t)$ was fit by Equation 8 the values of the residuals were smaller and had a flatter distribution.

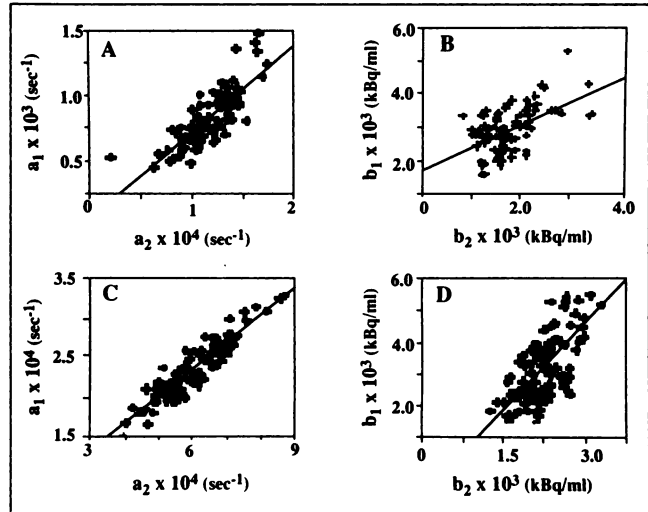


FIGURE 5. Correlation of parameters from fits of Equations 7 (A, B) and 8 (C, D) to all curves of $C_p(t)$ ($n = 119$). (A) Correlation between the two exponents (a_1 and a_2) from Equation 7. (B) Correlation between the two magnitude parameters (b_1 and b_2) from Equation 7. (C) Correlation between the two exponents (a_1 and a_2) from Equation 8. (D) Correlation between the two magnitude parameters (b_1 and b_2) from Equation 8. The two sets of coefficients determined by fitting Equation 8 (C, D) showed high correlation and, therefore, could be replaced by two coefficients without loss of accuracy.

$C_p(t)$ increased the s.d. of the percentage differences to over 9%. The increase in the s.d. explains why no satisfactory parameterization of the surfaces shown in Figure 3 could be found. The model implicit in that calculation ignores the effect of different values of the exponent “a.”

The percentage residuals for $C_x(T_i)$ calculated by analytic integration of Equation 9, as compared to the corresponding values obtained by numeric integration, had a mean (s.d.) of 0.9% (1.6%) for calculations of $C_1(T_i)$ and 0.33% (3.6%) for calculations of $C_2(T_i)$ (Fig. 7).

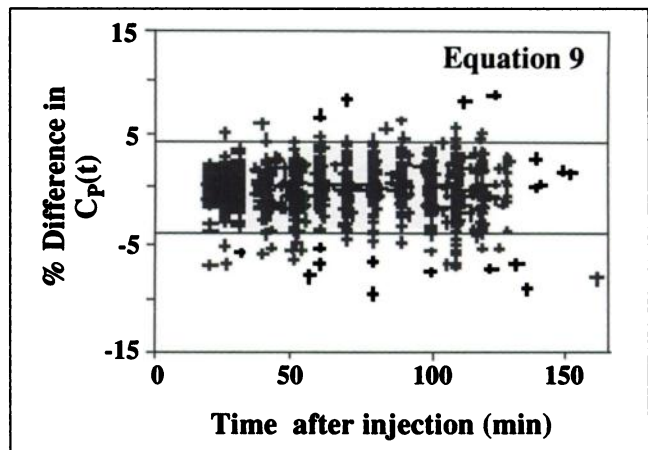


FIGURE 6. Percentage difference from fitting Equation 9 to $C_p(t)$. The area between the horizontal lines indicates the 95% confidence interval. The values of the s.d. (2.2%) agreed well with the value given by the counting statistics in the well counter.

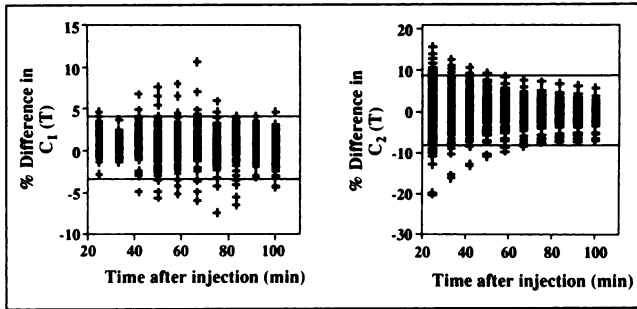


FIGURE 7. The ordinates show percentage differences in values of $C_1(T)$ (left) and $C_2(T)$ (right), calculated in two ways using Equation 3. The differences were obtained by subtracting the values obtained by analytic integration from those obtained by numeric integration.

Sensitivity to Peak $C_p(t)$

Calculation of $C_1(T)$ was insensitive to the peak $C_{p_n}(t)$, as shown by the absence of correlation ($r = 0.05$) (Fig. 8). In contrast, calculation of $C_2(T)$ was sensitive to the peak, as shown by the correlation coefficient of 0.60. Comparison of Figures 7B and 8B shows that the effect of peak height was only present for a relatively short time after injection. When $T > 45$ min the effect of peak height on values of $C_x(T)$ calculated using the modeled plasma curve was negligible.

The relationship between the magnitude of the percentage differences in values of $C_2(T_i)$ calculated by numeric integration versus analytic integration of Equation 9 and the peak value of $C_{p_n}(t)$ was not one of simple proportion. The curves with the largest values of peak $C_{p_n}(t)$ were not necessarily those with the largest differences between calculations of $C_2(T_i)$ made by numeric versus analytic techniques. The time and the shape (primarily the width) of the peak were also important. Curves of $C_{p_n}(t)$ with a peak occurring during the first 15–30 sec after FDG injection often had large positive differences, indicating that results of the analytic calculation were smaller than the results of the numeric calculation (Fig. 9A, B). Curves in which the peak occurred more than 1 min after FDG injection usually demonstrated negative differences (Fig. 9C, D). Since the observed differences were only appreciable for calculations

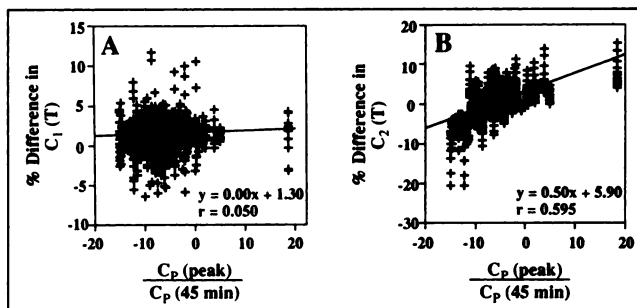


FIGURE 8. The ordinates show percentage differences in values of $C_1(T)$ (left) and $C_2(T)$ (right), calculated two ways using Equation 3. The differences were obtained by subtracting the values obtained by analytic integration from those obtained by numeric integration.

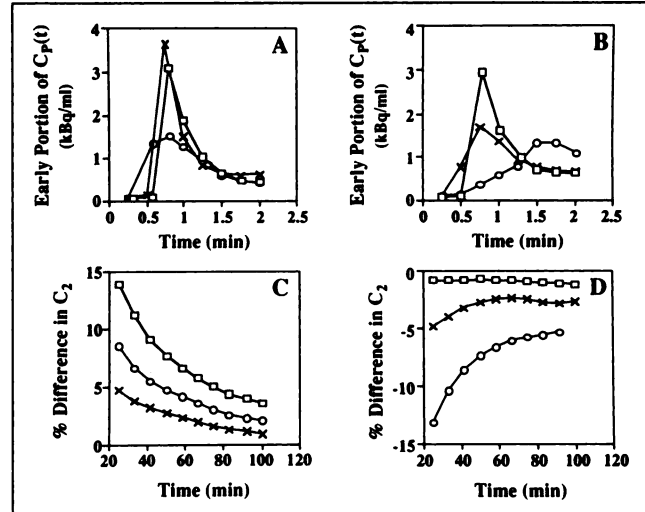


FIGURE 9. (A) Portions of three curves of $C_p(t)$. (B) Corresponding percentage differences between calculations of Equation 3 performed by numeric integration and by analytic integration using, as $C_p(t)$, Equation 9 with coefficients derived by fitting the equation to all samples of $C_p(t)$ with $t > 20$ min. The curves showed that the magnitudes of the percentage differences were not proportional to the value of peak $C_{p_n}(t)$ since the curve with the smallest peak had a difference midway between those from the curves with larger peak $C_{p_n}(t)$. (C) Portions of three curves of $C_{p_n}(t)$. (D) Corresponding percentage differences between calculations of Equation 3 performed by numeric integration and by analytic integration using, as $C_p(t)$, Equation 9 with coefficients derived by fitting the equation to all samples of $C_p(t)$ with $t > 20$ min.

in which the integration was performed to times $T < 45$ min, they could be ignored in calculations involving real PET scans.

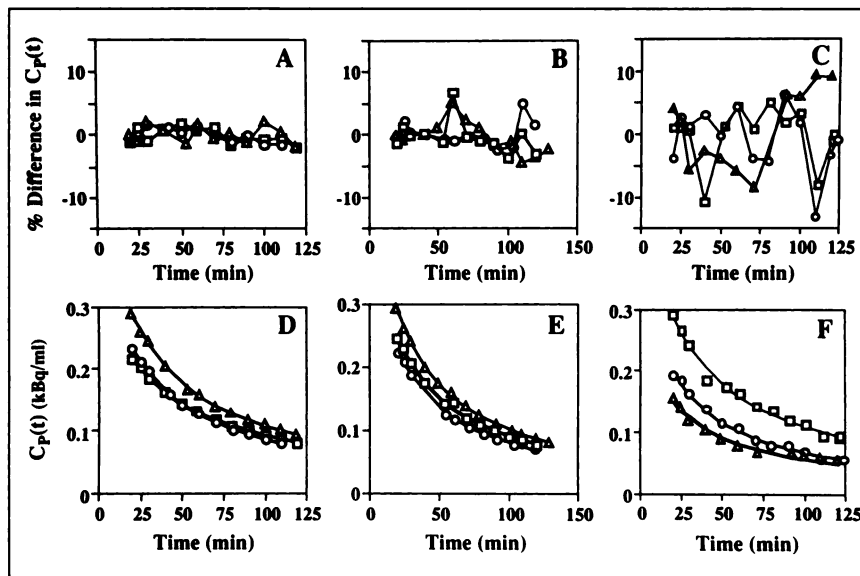
Some of the differences between values of $C_2(T)$ calculated by numeric integration and those calculated by analytic integration might have resulted from undersampling the curve of $C_p(t)$. The duration of the peak was generally less than 15 sec, as samples of $C_{p_n}(t)$ immediately preceding and following the sample with peak $C_{p_n}(t)$ generally had much less than half of the peak value. Some of the large differences were related to the technique for injection of FDG, particularly in those cases where the peak $C_{p_n}(t)$ occurred 1 min or more after the FDG injection was completed.

Sensitivity to Aberrant Samples

Most of the curves of $C_{p_n}(t)$ were fitted by Equation 9 with small, apparently random discrepancies (Fig. 10A, D). Some curves had samples that could not be fitted to the curve of Equation 9. These aberrant samples fell into one of three categories as follows: individual samples that had abnormally high or low levels of radioactivity compared to neighboring samples, pairs of samples whose order apparently had been switched and a block of samples that had lower activity than was expected of a smooth function (Fig. 10B, C, E, F). Ten of the 119 curves of $C_{p_n}(t)$ displayed one of these forms of aberration.

Another common problem with curves of $C_{p_n}(t)$ was

FIGURE 10. Examples of curves of $C_p(t)$ with and without aberrant samples. (A, B, C) Percentage difference in $C_p(t)$ between measured value compared to value calculated by fitting Equation 9 to all samples of $C_p(t)$. (D, E, F) $C_p(t)$ (symbols) and result of fitting Equation 9 (lines). (A, D) Typical curves of $C_p(t)$ showing good agreement. (B, E) Three curves of $C_p(t)$ showing individual aberrant samples. (C, F) The three curves with the largest disagreements in $C_p(t)$ between measured values and those obtained from the fitted curve.



missing data. This problem resulted from failure to draw scheduled samples (as commonly happened when the subject was being moved into the scanner). Missing a value of $C_{p_n}(t)$ resulted in a numeric integration calculation of $C_1(t)$ that was larger, by as much as 5%, than would have been calculated had the sample been present. The increase in the calculated value of $C_1(t)$ resulted from linear interpolation between samples of $C_{p_n}(t)$. Since the curve is always concave upward for $t > 20$ min, the interpolation always overestimates the value of $C_{p_n}(t)$ between samples.

Discrepancies between measured values of $C_{p_n}(t)$ and those calculated from the fitted curves were related to differences in the values of $C_1(T)$ calculated by numeric vs. by analytic integration. The discrepancies were directly proportional to the difference in $C_p(t)$ between measured and fitted values when $t = T$ (Fig. 11A), but not when $t \neq T$ (data not shown). The lack of correlation at other times demonstrated the dependence of $C_1(T)$ on only a few samples of $C_{p_n}(t)$, specifically those samples with $t \approx T$. Calculations of $C_2(T)$ were not sensitive to individual samples of $C_{p_n}(t)$ and, hence, showed no correlation with the variable on the abscissa of the plot, the difference between $C_{p_n}(t)$ and $C_p(t)$ calculated from the fitted function (Fig. 11B).

Number of Plasma Samples Required

Linear correlation coefficients were obtained among six sets of values of $C_x(T)$. The correlation coefficients were all greater than 0.9 (Table 3). The means of the percentage differences were all smaller than the standard deviations (data not shown). Therefore, the analytic calculations of $C_x(T)$ were not sensitive to the number of samples of $C_{p_n}(t)$ to which Equation 9 was fitted. The calculation also was not sensitive to the distribution in time of the samples.

Values of $C_x(T)$ in Set 1 were compared to values of $C_x(T)$ in Set 6. The mean (s.d.) of the percentage differences between the two sets of values of $C_1(T)$ was 0.003%

(2.1%) (Fig. 12A). The equivalent calculation for $C_2(T)$ revealed a mean (s.d.) of 0.55% (3.9%) (Fig. 12B). These results agreed well with those found in the comparison (above) of values of $C_x(T)$ in Set 1 to those in Set 2, which were determined based on fitting Equation 9 to all samples of $C_{p_n}(t)$ with $t > 20$ min.

Comparisons were performed between the values of $C_x(T)$ in Set 2 and those in Set 6. The standard deviations of the percentage residuals were 1.2% and 2.0% for calculations of $C_1(T)$ and $C_2(T)$, respectively (Fig. 12C, D). Thus the values of $C_x(T)$ in Set 6, which were based on only six samples of $C_{p_n}(t)$, were equivalent to the values of $C_x(T)$ in

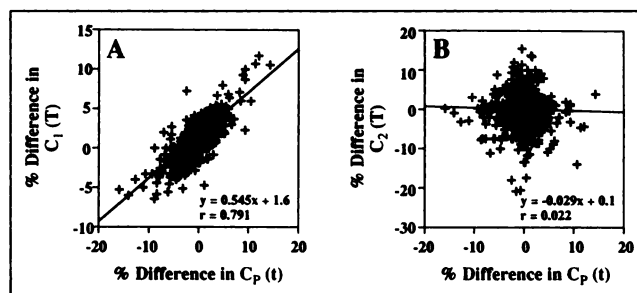


FIGURE 11. Ordinates show percentage differences in values of $C_1(T)$ (left) and $C_2(T)$ (right) calculated two ways using Equation 3. The differences were obtained by subtracting the values obtained by analytic integration from those obtained by numeric integration. The percentage differences between the analytic and numeric calculations of $C_1(T)$ are correlated with the percentage differences (or percentage residuals) from fitting Equation 9 to the samples of $C_p(t)$ ($r = 0.79$). Presence of a high correlation coefficient implies that the difference between the two calculations of $C_1(T)$ was due to the residual in the fit of $C_p(t)$. When the residuals in the fit of Equation 9 to $C_p(t)$ were small, then the differences in the two calculations of $C_1(T)$ were also small. In contrast, there was a low correlation coefficient between the differences in calculation of $C_2(T)$ and in the fit of Equation 9 to $C_p(t)$, therefore, the calculation was sensitive to samples of $C_p(t)$ other than those with $t \approx T$.

TABLE 3
Correlation Coefficients for Linear Correlation between $C_x(T)$ Values Calculated with Multiple Definitions for $C_p(t)$ Versus $C_x(T)$ Values Calculated with Several Possible Definitions for $C_p(t)$ *

Definition	$C_1(T)$					
	1	2	3	4	5	6
1	1.0000	0.9989	0.9998	0.9988	0.9992	0.9802
2	0.9989	1.0000	0.9989	0.9984	0.9982	0.9797
3	0.9998	0.9989	1.0000	0.9990	0.9991	0.9808
4	0.9988	0.9984	0.9990	1.0000	0.9979	0.9795
5	0.9992	0.9982	0.9991	0.9979	1.0000	0.9792
6	0.9802	0.9797	0.9808	0.9795	0.9792	1.0000

Definition	$C_2(T)$					
	1	2	3	4	5	6
1	1.0000	0.9918	0.9996	0.9987	0.9972	0.9270
2	0.9918	1.0000	0.9914	0.9914	0.9907	0.9192
3	0.9996	0.9914	1.0000	0.9991	0.9966	0.9279
4	0.9987	0.9914	0.9991	1.0000	0.9950	0.9215
5	0.9972	0.9907	0.9966	0.9950	1.0000	0.9237
6	0.9270	0.9192	0.9279	0.9215	0.9237	1.0000

*The six definitions for the function $C_p(t)$ in Equation 3 were as follows:

1. The measured values of $C_{p_n}(t)$ (using numeric integration).
2. Fitting Equation 9 to all samples of $C_{p_n}(t)$ with $t > 20$ min.
3. Fitting Equation 9 to samples used in item 2, removing the two samples with the largest residual from the fitting process, and refitting.
4. Fitting Equation 9 to the six earliest samples with $t > 20$ min, removing the two samples with the largest residuals and refitting.
5. Fitting Equation 9 to the six latest samples with $t > 20$ min, removing the two samples with the largest residuals and refitting.
6. Selecting six samples uniformly spaced in time with $20 \text{ min} < t < 90 \text{ min}$ and fitting to Equation 9, removing the two samples with the largest residuals and refitting.

The calculation of the values of $C_x(T)$ in Set 1 was performed using numeric integration, all the others used analytic integration. The correlation coefficients were > 0.9 for both results of calculations of $C_1(T)$ and $C_2(T)$. Furthermore, the means of the percentage residuals were all less than the corresponding standard deviations. Therefore, all six calculation methods produced equivalent results.

Set 2, which were based on all available samples of $C_{p_n}(t)$ with $t > 20$ min. The results of calculations of $C_x(T)$ in both Set 2 and Set 6 were equivalent to those in Set 1, which were based on numeric integration of all samples of $C_{p_n}(t)$.

DISCUSSION

The results demonstrate that CMRglc can be calculated from a small number of arterial plasma samples. The proposed technique uses six samples of $C_p(t)$, and provides a precision and accuracy of $\pm 5\%$ (95% confidence interval) of that achieved using the standard technique, which uses numeric integration of 30 or more values of $C_{p_n}(t)$. The use of six samples permits detection and removal of up to two aberrant samples during the fitting process. The proposed technique is less sensitive than the standard technique to missing or aberrant samples.

The high correlations between values of $C_x(T)$ and $C_p(t)$ proved that one could, in principle, calculate CMRglc using a single sample of $C_p(t)$. The correlations required only a standardization of t and T within each dataset, and were applicable for any t and T greater than 20 min. This finding supported and extended the findings that calculations of CMRglc based on using two samples of $C_p(t)$ to renormalize a population-average curve of $C_p(t)$ correlated well with values calculated by the conventional method (9). Nonetheless, calculation of CMRglc from only one or two samples of $C_p(t)$ can be influenced by aberrant samples, which can cause discrepancies of up to 20%. The presence of such samples in 10 of the 119 studies forced us to implement an algorithm that

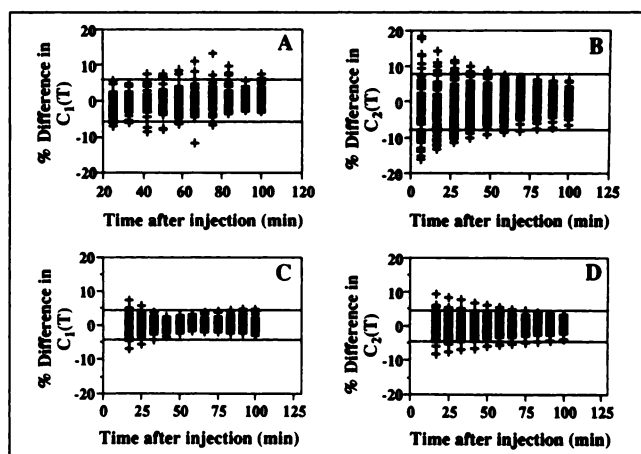


FIGURE 12. (A, B) The ordinates show percentage differences in values of $C_1(T)$ (A) and $C_2(T)$ (B) calculated two ways using Equation 3. (C, D) The ordinates show percentage differences in calculations of $C_1(T)$ (C) and $C_2(T)$ (D) by analytic integration of Set 6 versus Set 2 using Equation 3.

could detect and remove such samples from the analysis. In addition, we could discover no accurate and efficient parameterization of the equation required to calculate the values of $C_x(T)$ given a single value of $C_p(t)$ when the times (t and T) were arbitrary.

Using Equation 7 to fit the curve of $C_p(t)$ revealed two problems related to fitting a sum of exponentials to the time course of $C_p(t)$. The fit of $C_p(t)$ to the equation was not accurate, and the predictions of $C_x(T)$ varied with the selection of data points. Use of Equation 8 or 9 as a fitting function solved both of these problems.

Studies of the number of parameters showed that Equation 8 could be used to fit the curve of $C_p(t)$ using only two free parameters (Eq. 9). These studies relied on the high correlation between like parameters (i.e., a_1 was correlated with a_2 , and b_1 was correlated with b_2). The relationship of the pairs of parameters was represented as a proportion rather than just a linear correlation. Reducing the number of free parameters from four to two reduced the number of data points required to achieve stable predictions of $C_x(T)$.

Studies of the model showed that calculations based on one or two samples of $C_p(t)$ are vulnerable to variations in the shape of the curve of $C_p(t)$. The proposed technique is superior to using a curve shape derived by averaging a sample of such curves (9).

There is variation (approximately 10%) in the time course of $C_p(t)$, for which our procedure corrects by allowing the exponent "a" to vary. A fixed curve, of whatever shape, cannot account for such variation. The variation in curve shape represented by the variable "a" is one of the main reasons that no suitable parameterization could be found that would allow calculation of $C_x(T)$ from individual values of $C_p(t)$.

The set of data used in these analyses included plasma curves from subjects who experienced a range of perturbations in physical state including: changes in heart rate (primarily tachycardia due to cocaine and nicotine), hypercapnia (induced by morphine and breathing increased amounts of CO_2), decreased breathing rate (induced by morphine and buprenorphine), and others. None of these perturbations induced any conditions which invalidated or worsened the agreement of the model calculations with those of numeric integration. Had any such effect been present, there would have been outliers present in at least some of the figures.

The samples required for the proposed model are taken late in the procedure (i.e., 45 min or later after injection of FDG). At these times, measures of $C_{p_n}(t)$ taken from venous blood samples closely (within 2%) match those measured using arterial plasma samples (21). Therefore, the plasma samples required for analysis, using this method, might be taken from venous blood without loss of accuracy or precision.

CONCLUSION

A technique is proposed for estimating CMR_{glc} using single-scan FDG-PET. The technique requires only six

arterial plasma samples. To perform the most stable calculation of $C_x(T)$, plasma samples should be taken at 10–15-min intervals starting at least 30 min after injection of the radiotracer, thus obviating the need for sampling at 10–15-sec intervals. This technique has been shown to be valid over a wide range of physiological manipulations caused by administration of drugs of abuse. It is expected that the technique is valid in virtually any situation in which the static (or single-scan) FDG-PET measurement technique is valid. Further testing is required to determine if it is applicable to studies in which the subject undergoes glucose loading or elevation of insulin concentration in plasma.

ACKNOWLEDGMENTS

The authors thank Drs. R.F. Dannals and H. Ravert, who prepared the FDG, and D. Clough, CNMT and S. Herda, CNMT, who operated the PET scanner. They also gratefully thank Drs. R.A. Margolin, E.P.M. Broussolle, J.M. Stapleton, M.J. Morgan, N.G. Cascella, V.L. Villemagne, E.K. Shaya and S.F. Gilson for their contributions, as well as L.P. Rippetoe, RN, R. Stauffer, MS, RN, and M. Smith, RN, who participated in the data collection. The authors are deeply indebted to Drs. J.M. Links, D.B. Vaupel and S.J. Grant for their helpful discussions of the theory and presentation of our findings.

REFERENCES

- Sokoloff L, Reivich M, Kennedy C, et al. The [^{14}C]deoxyglucose method for the measurement of local cerebral glucose utilization: theory, procedure, and normal values in the conscious and anesthetized albino rat. *J Neurochem* 1977;28:897–916.
- Phelps ME, Huang SC, Hoffman EJ, Selin C, Sokoloff L, Kuhl DE. Tomographic measurement of local cerebral glucose metabolic rate in humans with (F-18)2-fluoro-2-deoxy-D-glucose: validation of method. *Ann Neurol* 1979;6:371–388.
- Huang S-C, Phelps ME, Hoffman EJ, Sideris K, Selin CJ, Kuhl DE. Non-invasive determination of local cerebral metabolic rate of glucose in man. *Am J Physiol* 1980;238:E69–E82.
- Huang SC, Phelps ME, Hoffman EJ, Kuhl DE. Error sensitivity of fluorodeoxyglucose method for measurement of cerebral metabolic rate of glucose. *J Cereb Blood Flow Metab* 1981;1:391–401.
- Reivich M, Alavi A, Wolf A, et al. Use of 2-deoxy-D[1- ^{11}C]glucose for the determination of local cerebral glucose metabolism in humans: variation within and between subjects. *J Cereb Blood Flow Metab* 1982;2:307–319.
- Kato A, Menon D, Diksic M, Yamamoto YC. Influence of the input function on the calculation of the local cerebral metabolic rate for glucose in the deoxyglucose method. *J Cereb Blood Flow Metab* 1984;4:41–46.
- Kuwabara H, Gjedde A. Measurements of glucose phosphorylation with FDG and PET are not reduced by dephosphorylation of FDG-6-phosphate. *J Nucl Med* 1991;32:692–698.
- Tamaki N, Yonekura Y, Kawamoto M, et al. Simple quantification of regional myocardial uptake on fluorine-18-deoxyglucose in the fasting condition. *J Nucl Med* 1991;32:2152–2157.
- Takikawa S, Dhawan V, Spetsieris P, et al. Noninvasive quantitative fluorodeoxyglucose PET studies with an estimated input function derived from a population-based arterial blood curve. *Radiology* 1993;188:131–136.
- Brooks RA. Alternative formula for glucose utilization using labeled deoxyglucose. *J Nucl Med* 1982;23:538–539.
- Hutchins GD, Holden JE, Koeppe RA, Halama JR, Gatley SJ, Nickles RJ. Alternative approach to single-scan estimation of cerebral glucose metabolic rate using glucose analogs, with particular application to ischemia. *J Cereb Blood Flow Metab* 1984;4:35–40.
- London ED, Cascella NG, Wong DF, et al. Cocaine-induced reduction of glucose utilization in human brain. A study using positron emission tomography and [fluorine-18]fluorodeoxyglucose. *Arch Gen Psychiatry* 1990;47:567–574.
- London ED, Broussolle EPM, Links JM, et al. Morphine-induced metabolic changes in human brain: Studies with positron emission tomography and [fluorine-18]fluorodeoxyglucose. *Arch Gen Psychiatry* 1990;47:73–81.

14. Walsh SL, Gilson SF, Jasinski DR, et al. Buprenorphine reduces cerebral glucose metabolism in polydrug abusers. *Neuropsychopharmacol* 1994;10:157-170.
15. Stapleton JM, Henningfield JE, Wong DF, et al. Effects of nicotine on cerebral metabolism and subjective responses in human volunteers [Abstract]. *Soc Neurosci Abstr* 1992;18:1074.
16. London ED, Margolin RA, Wong DF, et al. Cerebral glucose utilization in human heroin addicts: case reports from a positron emission tomographic study. *Res Commun Subst Abuse* 1989;10:141-144.
17. Brooks RA, Di Chiro G, Zukerberg BW, Bairamian D, Larson SM. Test-retest studies of cerebral glucose metabolism using fluorine-18 deoxyglucose: validation of method. *J Nucl Med* 1987;28:53-59.
18. Chang JY, Duara R, Barker W, Apicella A, Finn R. Two behavioral states studied in a single PET/FDG procedure: theory, method, and preliminary results. *J Nucl Med* 1987;28:852-860.
19. Chang JY, Duara R, Barker W, et al. Two behavioral states studied in a single PET/FDG procedure: error analysis. *J Nucl Med* 1989;30:93-105.
20. Hamacher K, Coenen HH, Stöcklin G. Efficient stereospecific synthesis of no-carrier-added 2-[¹⁸F]-fluoro-2-deoxy-D-glucose using aminopolyether supported nucleophilic substitution. *J Nucl Med* 1986;27:235-238.
21. Ohtake T, Kosaka N, Watanabe T, et al. Noninvasive method to obtain input function for measuring tissue glucose utilization of thoracic and abdominal organs. *J Nucl Med* 1991;32:1432-1438.

(continued from page 1552)

FIRST IMPRESSIONS: TESTICULAR LESIONAL UPTAKE OF TECHNETIUM-99M-MDP

PURPOSE

A 35-yr-old man with a history of osteomyelitis in the right upper femur was evaluated with ^{99m}Tc-methylene diphosphonate (MDP) scintigraphy. An anterior pelvic image showed increased activity in the right trochanter and a focus of activity in the left side of the scrotum, suggesting a testicular lesion (Fig. 1). A repeat image (Fig. 2) obtained after the patient changed clothes and washed the area resulted in a normal scrotal image, confirming urine contamination.

TRACER

Technetium-99m-MDP, 20 mCi (740 MBq)

ROUTE OF ADMINISTRATION

Intravenous

TIME AFTER INJECTION

2.5 hours

INSTRUMENTATION

GE Medical Systems Starcam 3200

CONTRIBUTORS

F. Tamgac, T. Akbunar and E. Alper, Uludag University School of Medicine, Bursa, Turkey

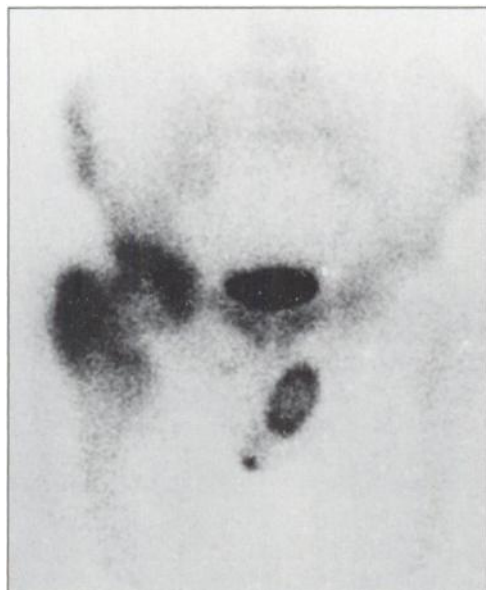


FIGURE 1.

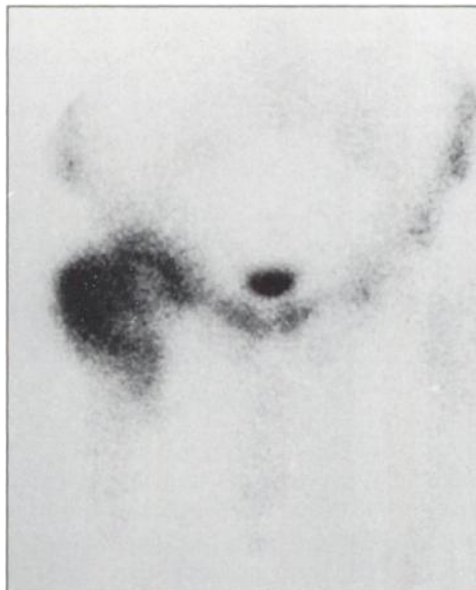


FIGURE 2.